RSC Advances

PAPER

View Article Online
View Journal | View Issue

Cite this: *RSC Adv.*, 2022, **12**, 3788

An organic–inorganic hybrid $K_2TiF_6 : Mn^{4+}$ red-emitting phosphor with remarkable improvement of emission and luminescent thermal stability†

Yan Yu,[a] Lin Wang,[a] Daishu Deng,[a] Xue Zhong,[a] Jiawei Qiang,[a] Tianman Wang,[a] Chunxiang Wu,[a] Sen Liao *[ab] and Yingheng Huang*[ab]

Received 30th November 2021
Accepted 15th January 2022

DOI: 10.1039/d1ra08734g

rsc.li/rsc-advances

A new type of monoethanolamine (MEA) and Mn^{4+} co-doped KTF : $MEAH^+$, Mn^{4+} (K_2TiF_6 : $0.1MEAH^+$, $0.06Mn^{4+}$) red emitting phosphor was synthesized by an ion exchange method. The prepared Mn^{4+} co-doped organic–inorganic hybrid red phosphor exhibits sharp red emission at 632 nm and the emission intensity at room temperature is 1.43 times that of a non-hybrid control sample KTF : Mn^{4+} (K_2TiF_6 : $0.06Mn^{4+}$). It exhibits good luminescent thermal stability at high temperatures, and the maximum integrated PL intensity at 150 °C is 2.34 times that of the initial value at 30 °C. By coating a mixture of KTF : $MEAH^+$, Mn^{4+}, a yellow phosphor (YAG : Ce^{3+}) and epoxy resin on a blue InGaN chip, a prototype WLED (white light-emitting diode) with CCT = 3740 K and R_a = 90.7 is assembled. The good performance of the WLED shows that KTF : $MEAH^+$, Mn^{4+} can provide a new choice for the synthesis of new Mn^{4+} doped fluoride phosphors.

1 Introduction

In recent years, WLEDs (white light-emitting diodes) with stable performance, energy saving, and outstanding luminescent characteristics have increasingly become an important requirement in the display and lighting fields.[1–5] At the moment, the commercially available WLEDs are composed of yellow emitting phosphors and blue emitting chips.[6] Although the device can produce white light, due to the lack of a red light component, its corresponding disadvantages are low color rendering index (R_a < 80) and high color temperature (CCT > 4500 K). So, it cannot well meet the requirements of the lighting field.[7] In order to obtain WLEDs with excellent performance, it is urgent to find a suitable red-emitting phosphor.

Among the many types of red phosphors, Mn^{4+} doped fluoride red phosphors have been widely reported due to their advantages such as high quantum efficiency at room temperature, effective absorption of near-UV and blue light, and narrow-band red light emission.[8–11] However, their inherent shortcoming is poor thermal stability of luminescence, and it is likely that the luminescent intensity will drop rapidly due to luminescent thermal quenching at high temperatures. Recently, a method to improve the luminous efficiency of inorganic phosphors is to graft with organic ligands, which can effectively promote the transfer of energy from the coordinated ligands to the activated ions, and results enhancement of the emission intensity.[12,13] And because organic–inorganic hybrid metal halide perovskite materials have good color tunability and high PLQE,[14,15] application of an organic–inorganic hybrid matrix for the synthesis of Mn^{4+} doped emitting phosphors has attracted the attention of some researchers. For example, T. Jüstel *et al.* reported an organic–inorganic hybrid $[C(NH_2)_3]_2GeF_6 : Mn^{4+}$ red phosphor that has narrow red emission at low temperatures (3 K) but exhibits severe luminescence quenching at room temperature.[16] Cai *et al.* reported an organic–inorganic hybrid $[(CH_3)_4]_2$-$TiF_6 : Mn^{4+}$ red phosphor can emission efficiently in the range of 50–300 K.[17] Although the above attempts are not satisfactory, they provide us with an idea to solve the problem of low luminescent thermal stability of red phosphors and to find new Mn^{4+} doped red phosphors.

Therefore, in order to synthesize a new type of Mn^{4+} doped fluoride red phosphor with excellent performances, we doped part of $MEAH^+$ in the K_2TiF_6 matrix, and synthesized Mn^{4+} doped KTF : $MEAH^+$, Mn^{4+} red phosphor on this basis. The prepared sample not only exhibits strong narrow red light emission at room temperature, but also exhibits strong negative luminescent thermal quenching, suggesting that the sample has great application prospects in WLEDs.

[a]*School of Chemistry and Chemical Engineering, Guangxi University, Nanning, Guangxi, 530004, China. E-mail: liaosen@gxu.edu.cn; liaosen380@hotmail.com; huangyingheng@163.com; Fax: +86 771 3233718; Tel: +86 771 3233718*

[b]*Guangxi Key Laboratory of Processing for Non-ferrous Metals and Featured Materials, School of Resources, Environment and Materials, Guangxi University, Nanning, Guangxi, 530004, China*

† Electronic supplementary information (ESI) available. See DOI: 10.1039/d1ra08734g

2 Experimental and methodology

The experiments and methodology are described in the ESI.†

3 Results and discussion

3.1 Structure, morphology and composition properties

Fig. 1 depicts the XRD patterns and FTIR spectra of samples (i–ii) and matrix. In Fig. 1(a), all diffraction peaks of the two samples are indexed in agreement with the standard data of space group PDF#08-0488 (pure hexagonal phase K_2TiF_6 with space group $P\bar{3}m1$), and the indexed results are listed in Table 1. The order of the lattice volume size of the samples is PDF#08-0488 > (ii) > (i). The ionic radii of Ti^{4+} and Mn^{4+} are 0.61 Å and 0.53 Å, respectively,[18] so the lattice volume will shrink when Mn^{4+} occupies the octahedral lattice sites of Ti^{4+}. The absence of any impurity peaks in the XRD patterns of KTF : $MEAH^+$, Mn^{4+} also show that $MEAH^+$ is doped into the KTF matrix. Fig. 1(b) shows that the 2θ angles of KTF : Mn^{4+} and KTF : $MEAH^+$, Mn^{4+} are both slightly shifted to a large angle. It indicates that the lattice volumes of both samples are slightly contracted and there is lattice distortion.

Fig. S1† shows the results obtained under natural light conditions using the ninhydrin method for KTF and KTF : 0.1$MEAH^+$ (KTF : $MEAH^+$), respectively. It can be seen from Fig. S1† that KTF does not change color, and KTF : $MEAH^+$ turns blue. In order to further confirm that $MEAH^+$ is doped into the lattice of the red phosphor, the infrared spectra of KTF : $MEAH^+$ and MEA were tested, and the corresponding infrared spectra were provided in Fig. 1(c). It is not difficult to see from Fig. 1(c) that some peaks of KTF : $MEAH^+$ show a slight red shift relative to MEA, but many peaks of the two can be matched. From the results, it can be concluded that $MEAH^+$ is indeed doped into the lattice of the matrix.

Fig. 2 shows the SEM images and EDS patterns of KTF : Mn^{4+} and KTF : $MEAH^+$, Mn^{4+}. Fig. 2(a) depicts that KTF : Mn^{4+} is composed of polyhedrons with a length of approximately 15 μm, and Fig. 2(b) depicts that KTF : $MEAH^+$, Mn^{4+} are composed of regular hexahedrons with a length of approximately 16–18 μm. The addition of $MEAH^+$ not only made the sample smooth, but also changed the morphology of KTF : $MEAH^+$, Mn^{4+}. Fig. 2(c) and (d) illustrate that KTF : Mn^{4+} is composed of K, Ti, F, and Mn elements, and KTF : $MEAH^+$, Mn^{4+} include K, Ti, F, Mn, C, O, and N elements. Since $MEAH^+$ contains C, O, and N elements, the results in Fig. 2(d) can indicate that $MEAH^+$ has successfully entered the K_2TiF_6 matrix.

Table 1 Refined lattice parameters of samples[a]

	$a = b$/Å	c/Å	$\alpha = \beta$/°	γ/°	V/Å^3
PDF#08-0488	5.7271	4.6619	90	120	132.4
(i)	5.723	4.65712	90	120	132.1
(ii)	5.72339	4.66014	90	120	132.2

[a] (i) KTF : Mn^{4+} and (ii) KTF : $MEAH^+$, Mn^{4+}.

3.2 Luminescent properties of room temperature

Fig. 3(a) and (b) show the luminescent characteristics of KTF : Mn^{4+} and KTF : $MEAH^+$, Mn^{4+}. It can be seen from Fig. 3(a) that the luminous intensity ratio of KTF : $MEAH^+$ and Mn^{4+}KTF : Mn^{4+} is 1.43, indicating that the luminous intensity of the former is enhanced by doping of $MEAH^+$. Fig. 3(a) and (b) indicate that the two samples have different emission and excitation bands, and the positions of the main peaks are almost the same. In the PLE spectra, there are two broad excitation bands centered at ~360 nm and ~460 nm, which originate from the $^4A_{2g} \rightarrow {}^4T_{1g}$ and $^4A_{2g} \rightarrow {}^4T_{2g}$ transitions of Mn^{4+} in octahedral symmetry, respectively. Under the excitation of 467 nm, the emission spectra have several sharp peaks in the range of 600–660 nm, of which the strongest peak is at 632 nm. They are attributed to the spin-forbidden d–d transition ($^2E_g \rightarrow {}^4A_{2g}$) of Mn^{4+}, and are activated by the $[MnF_6]^{2-}$ vibration mode.[19–22]

Fig. 3(c) depicts the lifetime curves of KTF : Mn^{4+} and KTF : $MEAH^+$, Mn^{4+}. They can be fitted by linear functions with constant terms. The lifetimes of the two samples are 5.68, 5.71 ms, respectively. It can be seen that the lifetime of KTF : $MEAH^+$, Mn^{4+} is improved after organic–inorganic hybridization. Theoretically, when energy transfer occurs between the donor and the acceptor, the lifetime of the donor

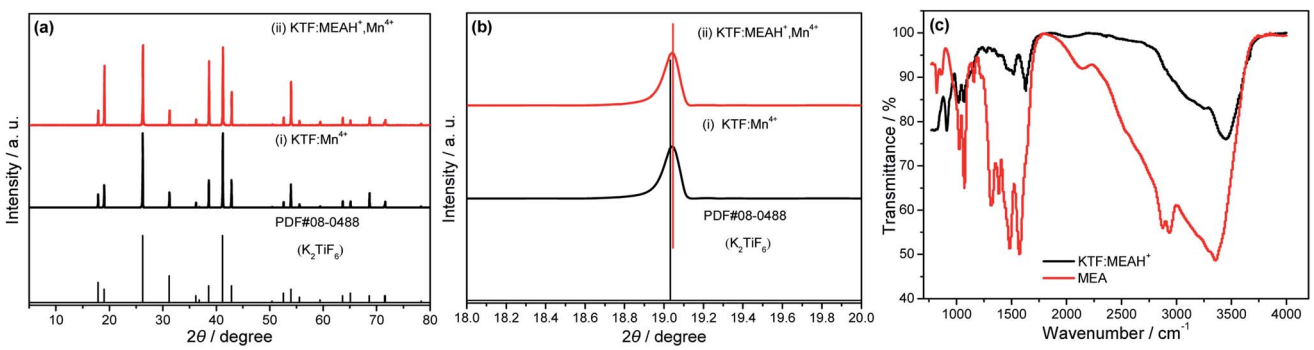

Fig. 1 XRD patterns and FTIR spectra of samples (i–ii) and matrix, (i) KTF : Mn^{4+} and (ii) KTF : $MEAH^+$, Mn^{4+}: (a) full XRD patterns, (b) expanded XRD patterns, (c) FTIR spectra of KTF : $MEAH^+$ and MEA.

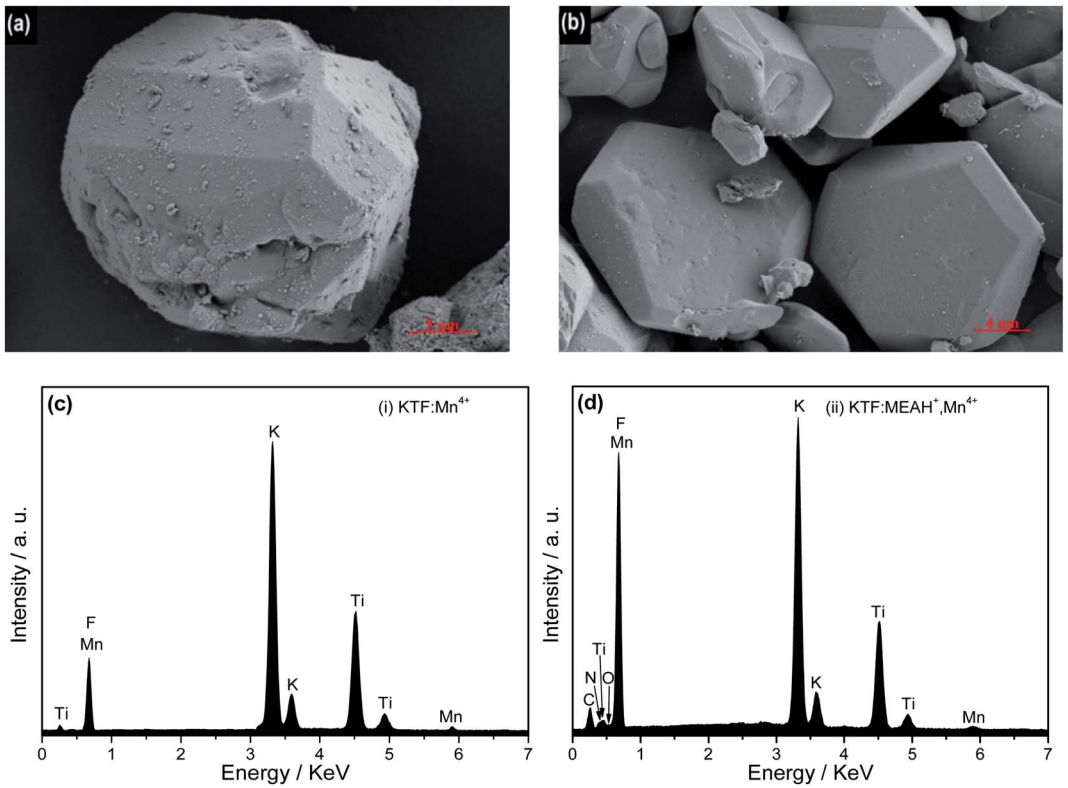

Fig. 2 SEM images and EDS spectra of two samples, (i) KTF : Mn^{4+} and (ii) KTF : $MEAH^{+}$, Mn^{4+}: (a and b) SEM images (c and d) EDS spectra.

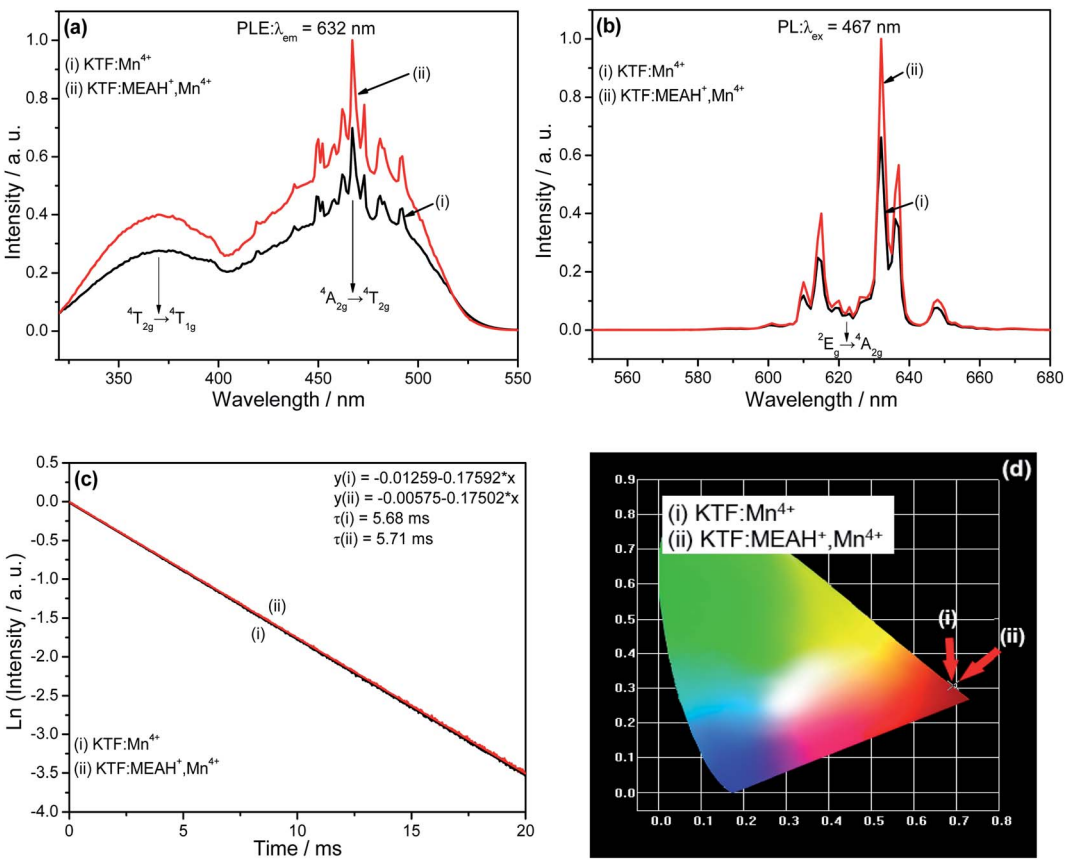

Fig. 3 Luminescent properties of two samples, (i) KTF : Mn^{4+} and (ii) KTF : $MEAH^{+}$, Mn^{4+}: (a) and (b) PLE and PL spectra of samples (i)–(ii), (c) decay curves, (d) CIE chromaticity diagram.

will decrease, and the lifetime of the acceptor will increase.[23] It is not difficult to see that the lifetimes of KTF : $MEAH^+$, Mn^{4+} are longer than the lifetime of KTF : Mn^{4+}, indicating that there is energy transfer from $MEAH^+$ (donor) to Mn^{4+} (acceptor).

The internal quantum yield (QY_i) values of KTF : Mn^{4+} and KTF : $MEAH^+$, Mn^{4+} are determined by eqn (S1).†[24–26] The QY_i of KTF : Mn^{4+} and KTF : $MEAH^+$, Mn^{4+} are determined to be 97.48 and 99.67%, respectively. The results of lifetime and QY_i show that luminescent performances can be enhanced by doping of $MEAH^+$.

Based on the emission spectra data in Fig. 3(b), the chromaticity coordinates of KTF : Mn^{4+} and KTF : $MEAH^+$, Mn^{4+} were calculated. The calculation results are shown in (Fig. 3(d)). The details are as follows: (a) KTF : Mn^{4+} is (0.6918, 0.3081), (b) KTF : $MEAH^+$, Mn^{4+} is (0.693, 0.3069).

Eqn (S2)† is used to calculate the color purity of the sample.[27–29] The calculated color purity values of KTF : Mn^{4+} and KTF : $MEAH^+$, Mn^{4+} are 99.57 and 99.93%, respectively.

3.3 Luminescent properties of different samples

The effect of different molar ratios (atomic ratios) of Mn^{4+} on the fluorescence properties of KTF : $MEAH^+$, xMn^{4+} (x = molar ratios of Mn/(Ti + Mn)) is shown in Fig. 4(a). The effect curve shown in Fig. 4(a) is a nonlinear curve with a maximum value. First of all, the curve increases with increasing x, reaching a maximum at $x = 0.06$, and decreases when x exceeds 0.06 due to quenching of the concentration.

Fig. 4(b) is the emission spectra of KTF : $y$$MEAH^+$, Mn^{4+} under different y (y = molar ratio of MEA/Ti, Mn^{4+} is fixed at 6%). The effect of y on the emission intensity is also a nonlinear curve with a maximum value. First, the emission intensity of this curve increases with the increase of y, and reaches the apex when $y = 10\%$, and then when $y > 10\%$, the emission intensity decreases due to the quenching of the concentration.

The quenching mechanism of Mn^{4+} concentration in KTF : $MEAH^+$, xMn^{4+} can be explored by calculating the critical distance (R_c) between Mn^{4+} ions. The eqn (S3)† is used to calculate R_c.[30]

For KTF : $MEAH^+$, Mn^{4+}, $V = 132.1$ Å^3, $x_c = 6\%$, and $N = 4$; R_c can be calculated as 10.17 Å. Since the R_c of the exchange interaction mechanism is less than 5 Å, and the current R_c is greater than 5 Å, suggesting that the quenching mechanism of Mn^{4+} concentration in KTF : $MEAH^+$, Mn^{4+} may not be an exchange interaction mechanism, but a multipolar interaction mechanism.

The related type of multipolar interaction can be determined according to the eqn (S4).†[30,31] Fig. 4(c) depicts that the dependence curve of Log(I/x) on Log(x) for KTF : $MEAH^+$, xMn^{4+} is a straight line with a slope of −1.4030. The slope corresponds to $\theta = 4.21$. Therefore, the quenching of Mn^{4+} concentration in the

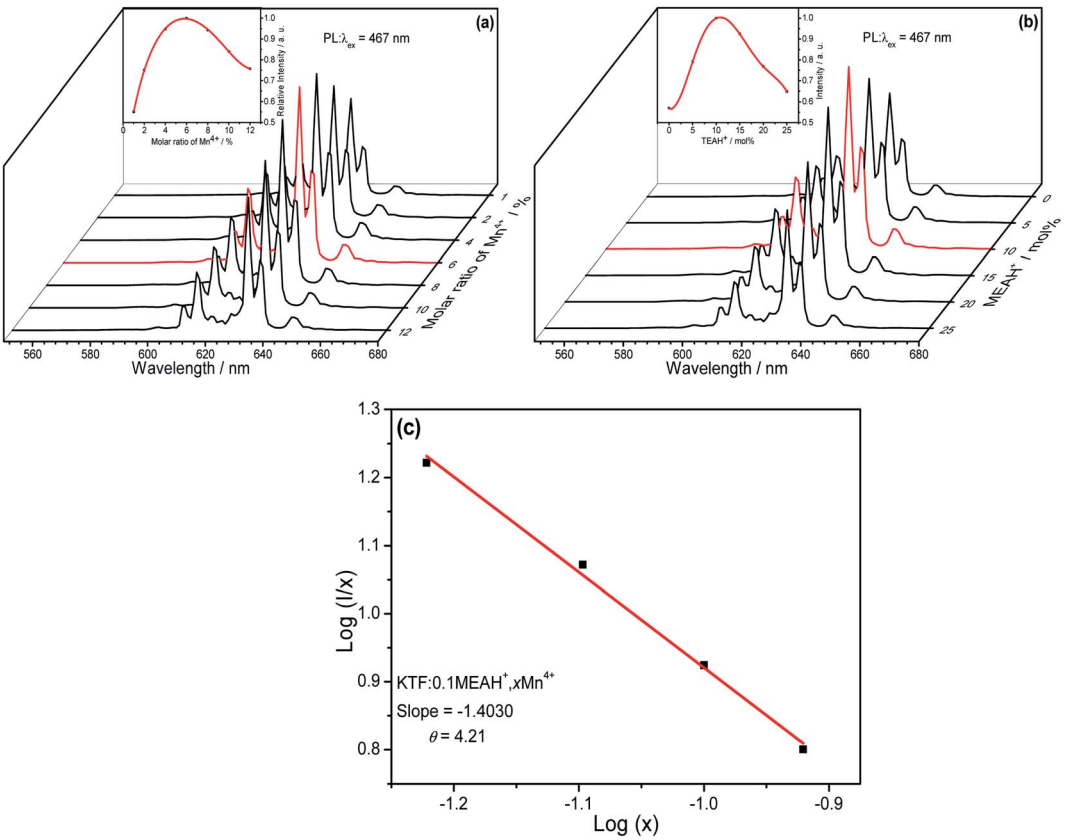

Fig. 4 The luminescent properties of KTF : 0.1$MEAH^+$, xMn^{4+} and KTF : $y$$MEAH^+$, 0.06$Mn^{4+}$ (a) and (b) PL spectra, (c) the related type line of multipolar interaction.

KTF : $MEAH^+$, xMn^{4+} sample can be identified as a mechanism of dipole–dipole interaction.

3.4 Analyses of thermal performances

Because the operating temperature of high-power LED devices may reach 150 °C, the luminescent thermal stability of phosphors is also an important evaluation index.[32] To compare the luminescent thermal stability of KTF : Mn^{4+} and KTF : $MEAH^+$, Mn^{4+} with commercial red phosphors, sample (0) CKTF : Mn^{4+} (commercial – K_2TiF_6 : $0.06Mn^{4+}$) was synthesized. The luminescent thermal stabilities of three samples were tested, and the results were depicted in Fig. 5(a–c). The PL spectrum intensities of the three samples are significantly affected by temperature. It is clear from Fig. 5(d) that the effect of temperature on the PL integrated intensities of all three samples are curves with a maximum value, indicating that the three samples all have negative thermal quenching (NTQ) effect. But, there is a huge difference between the three curves. Similar to results in many reports,[33–35] when the temperature increases, the PL integrated intensity of CKTF : Mn^{4+} only slightly increases, then reaches the maximum value at 90 °C, and the PL intensity is only 110% of its initial value at 30 °C. Unlike CKTF : Mn^{4+}, the integrated PL intensities of KTF : Mn^{4+} and KTF : $MEAH^+$, Mn^{4+} all reach the maximum at 150 °C. The maximum values of KTF : Mn^{4+} and KTF : $MEAH^+$, Mn^{4+} are 217 and 234% of their initial values at 30 °C, respectively. So, the strength order of the effect for the three samples is as follows: KTF : $MEAH^+$, Mn^{4+} > KTF : Mn^{4+} > CKTF : Mn^{4+}, indicating that KTF : Mn^{4+} and KTF : $MEAH^+$, Mn^{4+} have high luminescent thermal stability.

Regarding the mechanism of the NTQ effect, it has been reported that as the temperature increases, the extra energy of the electron traps formed from the matrix defects is transferred to Mn^{4+}, and leads to producing the effect.[36–38] So, the improvement mechanism of luminescent thermal stability for KTF : $MEAH^+$, Mn^{4+} can be attributed to increasing of electron traps induced by co-doping of $MEAH^+$.

Since CKTF : Mn^{4+}, KTF : Mn^{4+} and KTF : $MEAH^+$, Mn^{4+} are only different in the synthesis methods, but also in the NTQ effect, suggesting that it is our synthesized method that provide more suitable electron traps for KTF : Mn^{4+} and KTF : $MEAH^+$, Mn^{4+}.

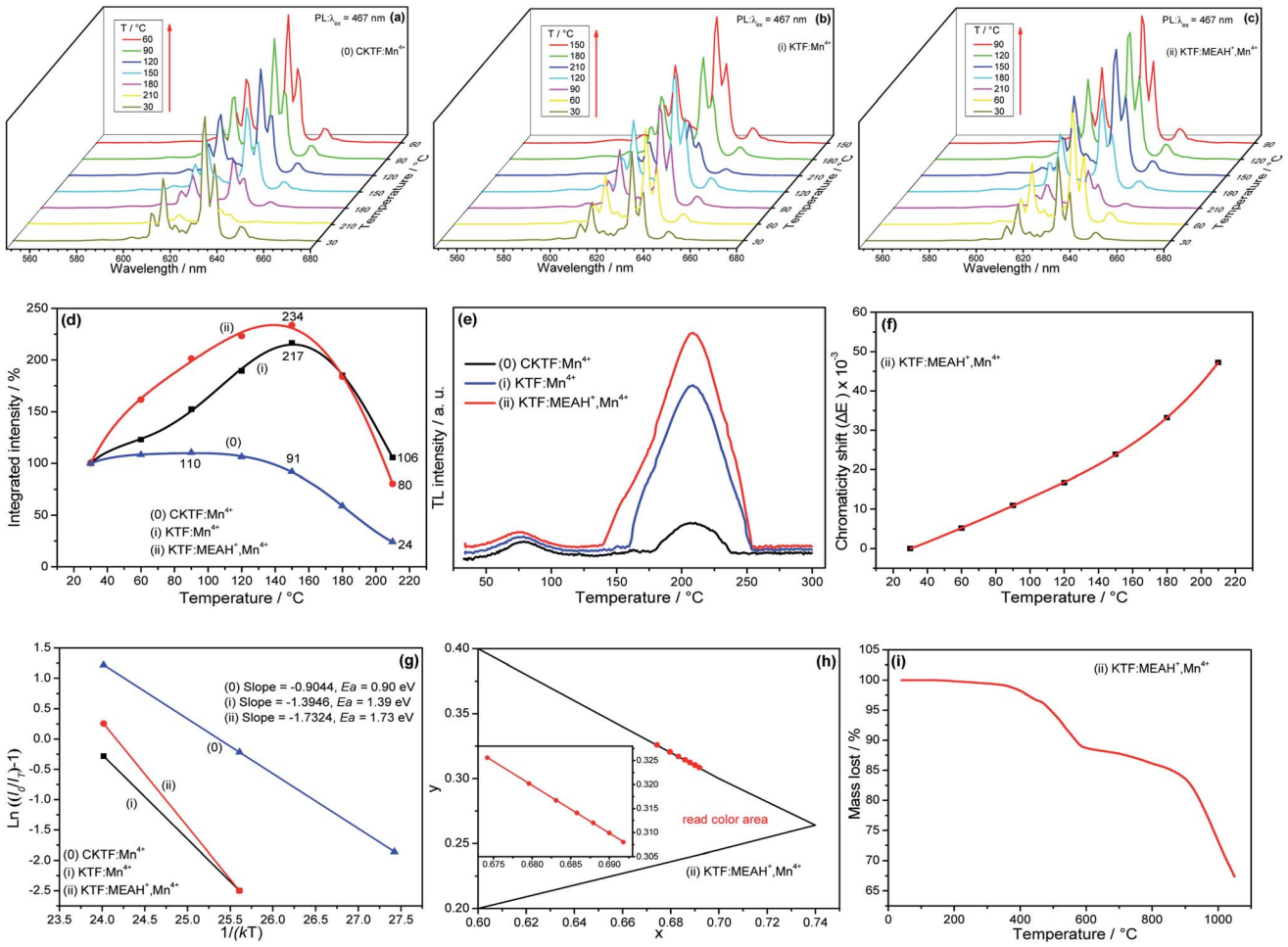

Fig. 5 Temperature-dependent PL performances of three samples, (0) CKTF : Mn^{4+}, (i) KTF : Mn^{4+} and (ii) KTF : $MEAH^+$, Mn^{4+}: (a)–(c) PL spectra; (d) integrated intensity curve; (e) thermo-luminescence curves; (f) chromaticity shift of sample (ii); (g) E_a curves; (h) CIE color coordinates of sample (ii); (i) TG of sample (ii).

In order to determine whether the doping of $MEAH^+$ can lead to the increase of the electron traps, we conducted thermoluminescence (TL) tests on CKTF : Mn^{4+}, KTF : Mn^{4+} and KTF : $MEAH^+$, Mn^{4+}. As shown in Fig. 5(e), there are mainly two traps located at 78 and 208 K in the TL curves. Compared with the trap depth of KTF : Mn^{4+}, the trap depth of KTF : $MEAH^+$, Mn^{4+} is larger, which may indicate that the doping of $MEAH^+$ can cause the increase of the electron traps.

In order to quantitatively describe the color stability, the eqn (S5)† is used to calculate the chromaticity shift (ΔE) of KTF : $MEAH^+$, Mn^{4+} at different temperatures.[39,40] As shown in Fig. 5(f), as the temperature increases, the chromaticity shift of KTF : $MEAH^+$, Mn^{4+} gradually increases. According to the curve, the ΔE of KTF : $MEAH^+$, Mn^{4+} at 175 °C is 31.56×10^{-3}, which is smaller than that of CSASNE (44×10^{-3}, at 175 °C). Because the smaller ΔE is, the more stable chromaticity is, the result indicates that KTF : $MEAH^+$, Mn^{4+} has high chromaticity stability and make it a potential phosphor for high-quality WLEDs.

To further understand the characteristics of luminescent thermal quenching, the eqn (S6)† is used to calculate E_a values of CKTF : Mn^{4+}, KTF : Mn^{4+} and KTF : $MEAH^+$, Mn^{4+}.[41,42] Using the slopes of the three straight lines in Fig. 5(g), the E_a values of the three samples can be calculated to be 0.90, 1.39 and 1.73, respectively. Since the larger E_a, the harder the luminescent thermal quenching occurs, so the order of luminescent thermal stability is KTF : $MEAH^+$, Mn^{4+} > KTF : Mn^{4+} > CKTF : Mn^{4+}.

Fig. 5(h) depicts the color coordinates of KTF : $MEAH^+$, Mn^{4+} at different temperatures. Fig. 5(h) shows that the color coordinates of KTF : $MEAH^+$, Mn^{4+} are only slightly shifted, showing that the color stability of KTF : $MEAH^+$, Mn^{4+} is high enough. The slight shift of the color coordinates may be resulted from the slight broadening of the PL peak.

To confirm the chemical thermal stability of KTF : $MEAH^+$, Mn^{4+}, TG measurement was performed. Fig. 5(i) depicts the TG curve of KTF : $MEAH^+$, Mn^{4+} from 40 °C to 1050 °C. From Fig. 5(i), it can be seen that KTF : $MEAH^+$, Mn^{4+} started to decompose at about 166 °C, indicating that KTF : $MEAH^+$, Mn^{4+} has good chemical thermal stability. The KTF : $MEAH^+$, Mn^{4+} has a relatively large mass loss from 360 °C, which is similar to our previous study.[43] In general, KTF : $MEAH^+$, Mn^{4+} is able to meet the requirements of WLEDs.

3.5 Performances of WLEDs

In order to evaluate the application potential of KTF : $MEAH^+$, Mn^{4+}, a mixture of KTF : $MEAH^+$, Mn^{4+}, YAG : Ce^{3+} and epoxy resin is coated on blue InGaN chips and assembled into prototype WLED. The performance of the WLED is shown in Fig. 6.

Fig. 6(a) is the electroluminescent spectrum of the WLEDs, which has blue, yellow and red emission bands. From the emission data of Fig. 6(a), the CIE chromaticity diagram (0.3773, 0.3332) in Fig. 6(b) can be acquired, and the color

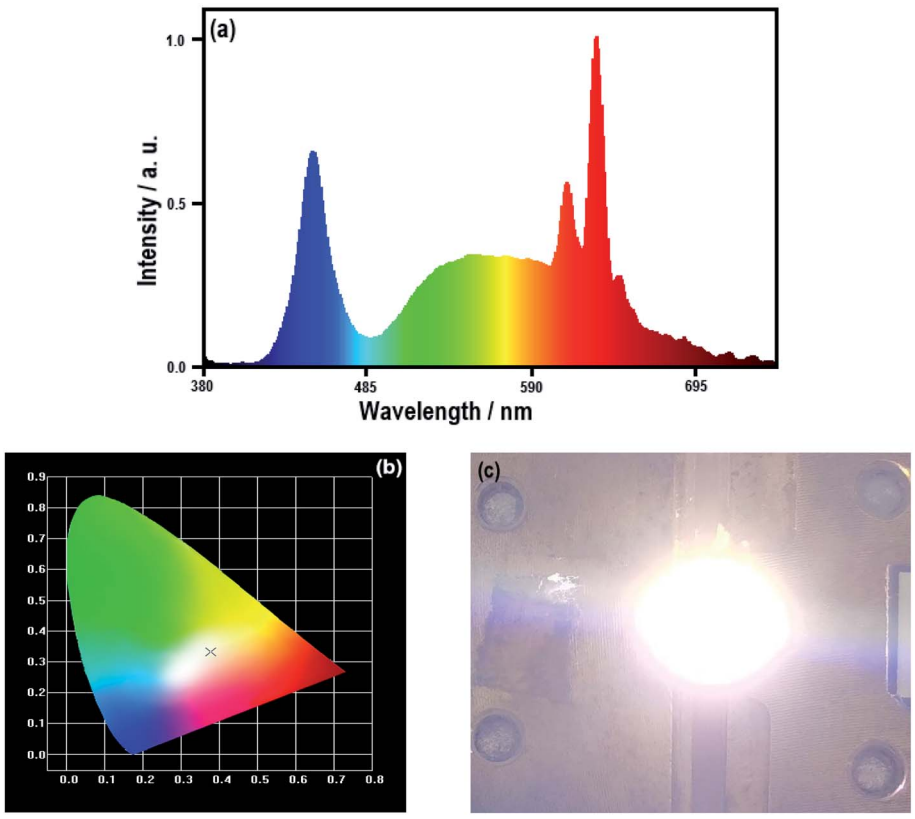

Fig. 6 Performances of prototype WLEDs using the mixing phosphors of KTF : $MEAH^+$, Mn^{4+} and YAG : Ce^{3+} based on InGaN chip under a 20 mA drive current: (a) electroluminescent spectra, (b) CIE chromaticity diagram, (c) luminescent photo.

coordinate point is in the white light region. Fig. 6(c) is a luminous photo, which shows warm white light. The results in Fig. 6(b) and (c) show that WLEDs emits good quality warm white light (CCT = 3740 K, R_a = 90.7).

4 Conclusions

In general, a new type of Mn^{4+} doped organic–inorganic hybrid KTF : $MEAH^+$, Mn^{4+} red emitting phosphor was synthesized by ion exchange method. By comparing KTF : Mn^{4+} and KTF : $MEAH^+$, Mn^{4+} in luminous intensity and QY_i, it can be found that KTF : $MEAH^+$, Mn^{4+} has high luminous intensity and nearly perfect quantum efficiency. The luminous intensity ratio of KTF : $MEAH^+$, Mn^{4+} and KTF : Mn^{4+} is 1.43, and the QY_i of KTF : $MEAH^+$, Mn^{4+} is 99.76%. When comparison of the thermal stability of CKTF : Mn^{4+} and KTF : $MEAH^+$, Mn^{4+}, where CKTF : Mn^{4+} was synthesized with a commercially available matrix, it can be found that at 150 °C, the integrated PL intensity of CKTF : Mn^{4+} is only 91% of its initial value, while the integrated PL intensity of KTF : $MEAH^+$, Mn^{4+} is 234% of its initial value. The results suggest that KTF : $MEAH^+$, Mn^{4+} is a red emitting phosphor with excellent luminescent thermal stability. By coating a mixture of KTF : $MEAH^+$, Mn^{4+}, YAG : Ce^{3+} and epoxy resin on a blue InGaN chip, prototype WLEDs with good warm white light (CCT = 3740 K, R_a = 90.7) were assembled. The results show that a new type of organic–inorganic hybrid red emitting phosphor has been successfully synthesized, which provides a new choice for the synthesis of red emitting phosphor.

Author contributions

Yan Yu: methodology, formal analysis, investigation, writing-original draft. Lin Wang: investigation. Daishu Deng: investigation. Xue Zhong: investigation. Jiawei Qiang: investigation. Tianman Wang: investigation. Chunxiang Wu: investigation. Sen Liao: conceptualization, supervision. Yingheng Huang: review & editing, visualization.

Conflicts of interest

There are no conflicts to declare.

Acknowledgements

This research is supported by the National Natural Science Foundation of China (Grant No. 21661006 and No. 21965004), the Natural Science Foundation of Guangxi Zhuang Autonomous Region, China (Grant No. 2019GXNSFDA245022, No. 2020GXNSFAA159036), the Scientific Research Foundation of Guangxi University (Grant No. XDZ140116), the Innovation Project of Guangxi Graduate Education (Grant No. YCSW2020015), the Students Experimental Skills and Innovation Ability Training Fund Project of Guangxi University (No. 202010593186).

References

1 Z. W. Jia, C. X. Yuan, Y. F. Liu, X. J. Wang, P. Sun, L. Wang, H. C. Jiang and J. Jiang, *Light: Sci. Appl.*, 2020, **9**, 86.
2 Z. Abbas, S. Azam, A. I. Bashir, A. Marriam, M. Waqas, T. Alshahrani and B. U. Haq, *Phys. Scr.*, 2020, **96**, 015801.
3 W. Xie, J. X. Li, C. X. Tian, Z. S. Wang, M. B. Xie, C. W. Zou, G. H. Sun and F. W. Kang, *Solid State Sci.*, 2018, **76**, 92–99.
4 J. Y. Wang, T. C. Lang, S. Q. Fang, T. Han, M. S. Cai, M. G. Wang, S. X. Cao, L. L. Peng, B. T. Liu, E. F. Polisadova and A. N. Yakovlev, *ACS Sustainable Chem. Eng.*, 2021, **9**, 2717–2726.
5 H. B. Nasrabadi, E. Madirov, R. Popescu, L. Štacková, P. Štacko, P. Klán, B. S. Richards, D. Hudry and A. Turshatov, *J. Mater. Chem. C*, 2021, **9**, 16313–16323.
6 Q. Yao, P. Hu, P. Sun, M. Liu, R. Dong, K. F. Chao, Y. F. Liu, J. Jiang and H. C. Jiang, *Adv. Mater.*, 2020, **32**, e1907888.
7 W. M. Ming, H. L. Shi and M. H. Du, *J. Mater. Chem. C*, 2018, **6**, 4171–4176.
8 Y. Y. Zhou, H. Ming, S. Zhang, T. T. Deng, E. H. Song and Q. Y. Zhang, *Chem. Eng. J.*, 2021, **415**, 128974.
9 D. X. Shi, Z. B. Liang, X. Zhang, Q. Zhou, Z. L. Wang, M. M. Wu and Y. Q. Ye, *J. Lumin.*, 2020, **226**, 117491.
10 S. Tang, Y. Liu, H. Li, Q. Zhou, K. M. Wang, H. J. Tang and Z. L. Wang, *J. Lumin.*, 2020, **224**, 117291.
11 J. M. Ha, E. Novitskaya, N. Lam, M. Sanchez, Y. H. Kim, Z. Z Li, W. B. Im, O. A. Graeve and J. McKittrick, *J. Lumin.*, 2020, **218**, 116835.
12 K. N. Narasimhamurthy, G. P. Darshan, S. C. Sharma, H. B. Premkumar, H. Adarsha and H. Nagabhushana, *J. Colloid Interface Sci.*, 2021, **600**, 887–897.
13 Q. Zhu, J. J. Liu, X. D. Li, X. D. Sun and J.-G. Li, *Appl. Surf. Sci.*, 2019, **489**, 142–148.
14 C. K. Zhou, Y. Tian, Z. Yuan, H. R. Lin, B. H. Chen, R. Clark, T. Dilbeck, Y. Zhou, J. Hurley, J. Neu, T. Besara, T. Siegrist, P. Djurovich and B. W. Ma, *ACS Appl. Mater. Interfaces*, 2017, **9**, 44579–44583.
15 M. Worku, L. J. Xu, M. Chaaban, A. Ben-Akacha and B. W. Ma, *APL Mater.*, 2020, **8**, 10902.
16 F. Baur, D. Böhnisch and T. Jüstel, *ECS J. Solid State Sci. Technol.*, 2020, **9**, 046003.
17 P. Q. Cai, S. Wang, T. M. Xu, Y. Tang, X. L. Yuan, M. J. Wan, Q. Ai, J. J. Si, X. Yao, Y. G. Cao, M. K. Rabchinskii, P. N. Brunkov and Z. G. Liu, *J. Lumin.*, 2020, **228**, 117661.
18 H. M. Zhu, C. C. Lin, W. Q. Luo, S. T. Shu, Z. G. Liu, Y. S. Liu, J. T. Kong, E. Ma, Y. G. Cao, R. S. Liu and X. Y. Chen, *Nat. Commun.*, 2014, **5**, 4312.
19 H. H. Zhang, Y. Y. Chen, X. Y. Zhu, K. L. Liu, H. C. Zhou, X. K. Sun, N. N. Li and Y. L. Feng, *J. Lumin.*, 2021, **236**, 118131.
20 Y. J. Wang, C. K. Yu, Y. Y. Zhou, E. H. Song, H. Ming and Q. Y. Zhang, *J. Alloys Compd.*, 2021, **855**, 157347.
21 L. P. Dong, L. Zhang, Y. C. Jia, B. Q. Shao, W. Lü, S. Zhao and H. P. You, *ACS Sustainable Chem. Eng.*, 2020, **8**, 3357–3366.
22 T. C. Lang, J. Y. Wang, T. Han, M. S. Cai, S. Q. Fang, Y. Z. Zhong, L. L. Peng, S. X. Cao, B. T. Liu, E. Polisadova,

V. Korepanov and A. Yakovlev, *Inorg. Chem.*, 2021, **60**, 1832–1838.
23 W. Li, H. R. Zhang, S. Chen, Y. L. Liu, J. L. Zhuang and B. F. Lei, *Adv. Opt. Mater.*, 2016, **4**, 427–434.
24 J. Wu, Z. Y. Li, L. Luo, Y. H. Xiong, L. Y. Jiang, R. Guo and L. L. Meng, *J. Alloys Compd.*, 2021, **863**, 158058.
25 L. Q. Xi, Y. X. Pan, M. M. Zhu, H. Z. Lian and J. Lin, *Dalton Trans.*, 2017, **46**, 13835–13844.
26 L. Shi, Y. J. Han, Z. X. Ji and Z. W. Zhang, *J. Mater. Sci.: Mater. Electron.*, 2019, **30**, 3107–3113.
27 L. Y. Wang, E. H. Song, Y. Y. Zhou, T. T. Deng, S. Ye and Q. Y. Zhang, *J. Mater. Chem. C*, 2017, **5**, 7253–7261.
28 W. Li, L. L. Sun, B. Devakumar, N. Ma, Z. J. Zhang and X. Y. Huang, *J. Photochem. Photobiol., A*, 2021, **410**, 113166.
29 M. M. Zhu, Y. X. Pan, L. Q. Xi, H. Z. Lian and J. Lin, *J. Mater. Chem. C*, 2017, **5**, 10241–10250.
30 L. F. Yuan, Y. H. Jin, G. T. Xiong, H. Y. Wu, J. C. Li, H. Liu, L. Chen and Y. H. Hu, *J. Alloys Compd.*, 2021, **870**, 159394.
31 N. Ma, W. Li, B. Devakumar, S. Y. Wang, L. L. Sun, Z. J. Zhang and X. Y. Huang, *J. Lumin.*, 2021, **233**, 117901.
32 L. Huang, Y. W. Zhu, X. J. Zhang, R. Zou, F. J Pan, J. Wang and M. M. Wu, *Chem. Mater.*, 2016, **28**, 1495–1502.
33 Y. W. Zhu, Y. Liu, L. Huang, T. T. Xuan and J. Wang, *Sci. China: Technol. Sci.*, 2017, **60**, 1458–1464.
34 L. Y. Wang, E. H. Song, T. T. Deng, Y. Y. Zhou, Z. F. Liao, W. R. Zhao, B. Zhou and Q. Y. Zhang, *Dalton Trans.*, 2017, **46**, 9925–9934.
35 M. M. Zhu, Y. X. Pan, X. A. Chen, H. Z. Lian and J. Lin, *J. Am. Ceram. Soc.*, 2018, **101**, 4983–4993.
36 S. Q. Fang, T. C. Lang, T. Han, J. Y. Wang, J. Y. Yang, S. X. Cao, L. L. Peng, B. T. Liu, A. N. Yakovlev and V. I. Korepanov, *Chem. Eng. J.*, 2020, **389**, 124297.
37 X. T Fan, W. B. Chen, S. Y. Xin, Z. C. Liu, M. Zhou, X. Yu, D. C. Zhou, X. H. Xu and J. B. Qiu, *J. Mater. Chem. C*, 2018, **6**, 2978–2982.
38 W. Q. Xie, P. P. Li, Y. Wang, Q. J. Zhu, Y. J. Zhang, Y. J. Cai, S. Q. Xu and J. J. Zhang, *J. Mater. Chem. C*, 2019, **7**, 8655–8659.
39 F. Hong, G. Pang, L. J. Diao, Z. D. Fu, G. X. Liu, X. T. Dong, W. S. Yu and J. X. Wang, *Dalton Trans.*, 2020, **49**, 13805–13817.
40 Y. Y. Liu, J. Gao, W. Shi, X. Y. Feng, Z. J. Zhou, J. X. Wang, J. L. Guo, R. Y. Kang, B. Deng and R. J. Yu, *Ceram. Int.*, 2021, **47**, 18814–18823.
41 Y. W. Zhu, L. Huang, R. Zou, J. H. Zhang, J. B. Yu, M. M. Wu, J. Wang and Q. Su, *J. Mater. Chem. C*, 2016, **4**, 5690–5695.
42 P. Xue and L. H. Tian, *Opt. Mater.*, 2021, **115**, 111063.
43 Y. M. Liu, T. M. Wang, Z. P. Chen, K. Y. Chen, M. M. Guan, Y. H. Huang, S. Liao and H. X. Zhang, *J. Mater. Sci.: Mater. Electron.*, 2018, **29**, 12536–12542.